Surface chemistry of black phosphorus under a controlled oxidative environment

2016 Nanotechnology 27 434002

(http://iopscience.iop.org/0957-4484/27/43/434002)

IOP Publishing Nanotechnology
Nanotechnology 27 (2016) 434002 (10pp) doi:10.1088/0957-4484/27/43/434002

Surface chemistry of black phosphorus under a controlled oxidative environment

Wei Luo[1,2,3], Dmitry Y Zemlyanov[2,4], Cory A Milligan[2], Yuchen Du[2,3], Lingming Yang[2,3], Yanqing Wu[1] and Peide D Ye[2,3,4]

[1] School of Electrical and Electronic Engineering, Huazhong University of Science and Technology, Wuhan 430074, People's Republic of China
[2] Birck Nanotechnology Center, Purdue University, West Lafayette, IN 47907, USA
[3] School of Electrical and Computer Engineering, Purdue University, West Lafayette, IN 47907, USA

E-mail: dimazemlyanov@purdue.edu and yep@purdue.edu

Received 4 May 2016, revised 22 August 2016
Accepted for publication 26 August 2016
Published 23 September 2016

Abstract

Black phosphorus (BP), the bulk counterpart of monolayer phosphorene, is a relatively stable phosphorus allotrope at room temperature. However, monolayer phosphorene and ultra-thin BP layers degrade in ambient atmosphere. In this paper, we report the investigation of BP oxidation and discuss the reaction mechanism based on the x-ray photoelectron spectroscopy (XPS) data. The kinetics of BP oxidation was examined under various well-controlled conditions, namely in 5% O_2/Ar, 2.3% H_2O/Ar, and 5% O_2 and 2.3% H_2O/Ar. At room temperature, the BP surface is demonstrated not to be oxidized at a high oxidation rate in 5% O_2/Ar nor in 2.3% H_2O/Ar, according to XPS, with the thickness of the oxidized phosphorus layer <5 Å for 5 h. On the other hand, in the O_2/H_2O mixture, a 30 Å thickness oxide layer was detected already after 2 h of the treatment. This result points to a synergetic effect of water and oxygen in the BP oxidation. The oxidation effect was also studied in applications to the electrical measurements of BP field-effect transistors (FETs) with or without passivation. The electrical performance of BP FETs with atomic layer deposition (ALD) dielectric passivation or h-BN passivation formed in a glove-box environment are also presented.

Keywords: black phosphorus, phosphorene, XPS, ALD, FET, passivation

(Some figures may appear in colour only in the online journal)

1. Introduction

The research area of 2D semiconducting crystals has been really booming in the past several years, due to their promising characteristics for electronic and optoelectronic applications. Since the layers of 2D materials bind through weak van der Waals force, monolayer and/or ultra-thin films can be experimentally produced by standard scotch tape exfoliation. Black phosphorus (BP) is an emerging 2D material which attracts wide attention. BP has high carrier mobility with a finite direct band gap, varying from 0.3 eV in bulk form up to 1.5–2.0 eV in monolayer phosphorene [1–6]. The synthesis, physical properties, and device applications of bulk BP have been investigated to some extent [7–12]. The superior transport properties of ultra-thin BP films have attracted wide interest and attention from the physics, chemistry and device communities [13–20], because BP has bridged the gap between gapless graphene and wide bandgap transition metal dichalcogenides (TMDs).

BP, the bulk counterpart of phosphorene, is a relatively stable phosphorus allotrope at room temperature. However, phosphorene and ultra-thin BP films are less firm in air under atmospheric conditions and their future applications for microelectronic devices require developing protection methods and dielectric covering techniques. A few approaches were proposed such as boron nitride (h-BN) passivation [17–20], organic polymer coating [21], and atomic layer deposition (ALD) dielectric capping [22, 23]. The h-BN passivation seems to provide a better 2D–2D interface on BP eliminating surface scattering. Nevertheless, it is not easy to scale the

[4] Authors to whom any correspondence should be addressed.

'flake-to-flake' transfer technique to a large-area wafer-size manufacturing technology. Organic polymers might provide only short-time protection: degradation of flake quality with time has been reported [1]. ALD seems to be promising, but the challenge is to develop the ALD process for BP minimizing the damaging effect by an organometallic precursor and ALD oxidant (water, oxygen, ozone, etc). To understand the degradation mechanism of BP, detailed studies of individual reactions are needed. Previous research had focused on the degradation process of BP in ambient atmosphere [22–27]. However, the contributions and effects of the different oxidants are still not clear. In this paper, we report the systematic study of the kinetics of the BP oxidation under different oxidative environments. BP was exposed to 5% O_2/Ar, 2.3% H_2O/Ar, and 5% O_2 and 2.3% H_2O/Ar at room temperature and atmospheric pressure and the surface composition was characterized by x-ray photoelectron spectroscopy (XPS). A reaction cell, where the sample was treated, was directly attached to the XPS instrument, and the transfer was done under ultra-high vacuum (UHV) without contact with air, avoiding possible contamination and uncontrolled oxidation. The key result is that neither water nor oxygen alone is a strong oxidant of BP, but a mixture of O_2/H_2O results in much faster oxidation. Electrical measurements on BP-based devices prepared using two different ALD protocols demonstrate that the device, which had less contact with water, shows better electrical performance than the one exposed to moisture. Similarly, BP devices with h-BN passivation retain the high performance for a long period of time, compared to the naked devices. The goal of this paper is to give guidance on how to preserve a BP surface providing a moisture-free environment as well as smart engineering of ALD integration using water-free precursors as oxidants.

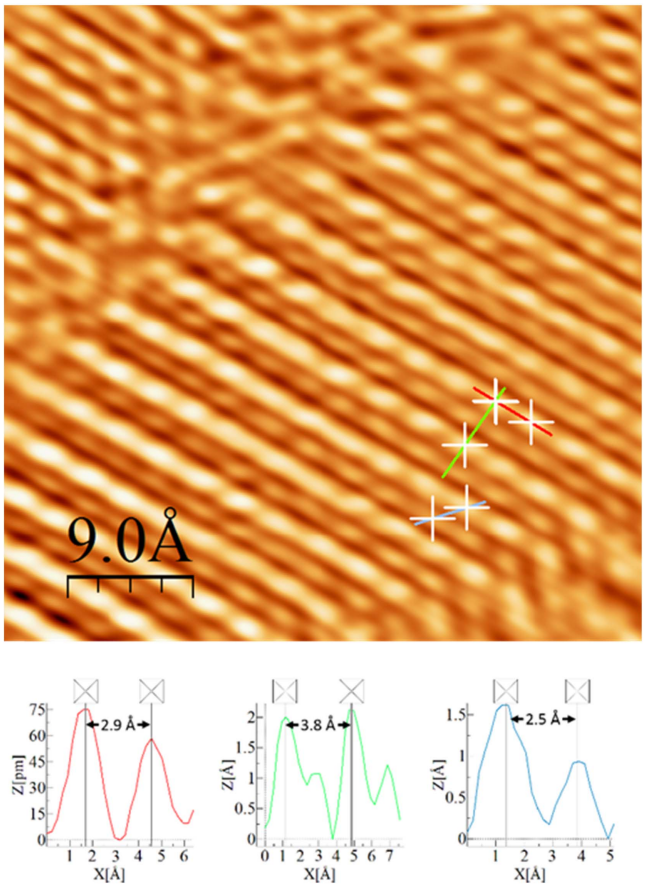

Figure 1. STM image (4.5 × 4.5 nm) of a BP surface after shaving a bulk BP crystal. The unit cell base vectors are denoted by the red and green solid lines. The atomic distance between the phosphorous atoms in the zigzag chain is denoted by the blue line. Scanning parameters: U_{bias} = 0.3 V, $I_{tunneling}$ = 1.1 nA. The images were obtained at room temperature.

2. Experimental methods

2.1. XPS, STM analysis and sample preparation

XPS data were obtained with a Kratos Axis Ultra DLD spectrometer using monochromatic Al Kα radiation (hν = 1486.58 eV). Survey and high-resolution spectra were collected at a fixed analyzer pass energy of 160 and 20 eV, respectively. The acquisition was performed at photoemission angles of 0° measured with respect to the surface normal, where binding energy (BE) values were directly referenced to the Fermi edge. All spectra were corrected by setting the P $2p_{3/2}$ peak at 130.0 eV, and the BE scale of the XPS instrument was calibrated using Au $4f_{7/2}$ = 84.00 eV and Cu $2p_{3/2}$ = 932.67 eV as the reference. The spectrometer resolution, measured as a full width at half maximum (FWHM) of the P 2p peaks was 0.45 eV. All spectra were analyzed using the CasaXPS software program, version 2.3.16 Pre-rel 1.4 from Casa Software Ltd. The curve fitting was performed after linear or Shirley-type background subtraction assuming a Gaussian/Lorentzian peak shape. In addition, all P 2p peaks were fitted as a spin–orbit splitting doublet with a separation of 0.85 eV, and the intensity ratio between P $2p_{3/2}$ and P $2p_{1/2}$ was fixed to be 2:1.

A BP piece was first mounted on a stainless steel XPS holder and the sample was cleaved in an Ar-filled glove box, which is directly attached to a load-lock of the XPS spectrometer. The oxygen and water level in the glove box was less than 0.1 ppm. The freshly cleaved BP sample was immediately transferred to the UHV XPS chamber without contact to air. Sample treatments were performed in a reaction cell (~30 cm^3) also connected to the XPS spectrometer. The BP samples were moved between the reaction cell and the analysis chamber under UHV conditions without contact to air. The BP samples were treated in three different oxidative environments, 5% O_2/Ar, 2.3% H_2O/Ar, and 5% O_2 and 2.3% H_2O/Ar, at the temperature of 20 °C under atmospheric pressure in a constant flow regime of 100 sccm. The gas flow and compositions were controlled by mass-flow controllers. Only ultra-high purity gases (O_2, Ar) were used (99.99%). The water vapor was obtained by passing the gas mixture through a room-temperature water saturator with the total organic carbon (TOC) reduced from 1 to 0.25 ppb.

The high-quality of the starting BP surface is the key for reliable XPS study and is confirmed by the scanning

tunneling spectroscopy (STM) studies, as shown in figure 1. The atomically resolved fresh BP surface can be retained in UHV for a long time to perform the XPS studies. The atomic arrangement in figure 1 is identical to those reported in [28]. This structure was assigned to the BP (010) surface. The length of a and c is 3.8 Å as denoted by the green lines in figure 1 and 2.9 Å as denoted by the red lines, being consistent with the literature values. The two topmost atoms (2.5 Å apart, the blue lines in figure 1) in an 'arm-chair' have different electronic structure. This results in these two atomic rows. The one is lower and the other is higher, as can be seen at the bias of 0.3 eV. The typical size of the (010) terraces was approximately 3 nm and the STM image demonstrates the boundary between the (010) terraces on the top left and the bottom right corners. The STM images were collected using an Omicron ambient temperature UHV STM/AFM system with electrochemically etched W tips at constant-current topographic mode. The bias varied between +0.1 V and +1.0 V with tunnel currents ranging from +0.1 to +2.5 nA. In all experiments reported here, the sample was electrically grounded.

2.2. XPS data quantification

We have used Fadley's approach for the XPS data quantification [29]. Atomic percentages of elements are typically reported as a quantifying value, because of its simplicity. However, this approach works for the homogeneously mixed elements and chemical states and this is not a case for the flat sample and the surface oxidation. Therefore, we used the coverage and thickness of the oxide layer as quantification parameters. The coverage was measured in monolayer, ML, which is the ratio between the numbers of the adsorbed species and the surface atoms. The coverage was calculated by assuming a non-attenuating overlayer on a semi-infinite substrate at fractional coverage [29] as:

$$\Theta = \frac{N_{\mathrm{overl}}(\theta) \times \frac{\mathrm{d}\sigma_s}{\mathrm{d}\Omega} \times \Lambda_e^{\mathrm{subst}}(E_{\mathrm{subst}}) \times \cos\theta}{N_{\mathrm{subst}}(\theta) \times \frac{\mathrm{d}\sigma_{\mathrm{overl}}}{\mathrm{d}\Omega} \times d_{\mathrm{subst}}} \quad (1)$$

where $N_{\mathrm{overl}}(\theta)$ and $N_{\mathrm{subst}}(\theta)$ are the intensities (areas) of the characteristic photoemission peaks of the oxidized layer and substrate, correspondently; $\frac{\mathrm{d}\sigma}{\mathrm{d}\Omega}$ is the differential cross-section for the photoemission peaks of substrate (P 2p) and oxidized layer (O 1s), which can be calculated from Scofield cross-sections [30] and the Reilman asymmetry parameter [31], $\Lambda_e^{\mathrm{subst}}(E_{\mathrm{subst}})$ is the electron attenuation length of an electron originated from substrate traveling through a substrate, and θ is the photoemission angle of electron relative to the surface normal.

Thickness of the oxidized layer, t, was calculated assuming a semi-infinite substrate with a uniform thickness overlayer using [29]:

$$\frac{N_{\mathrm{overl}}(\theta)}{N_{\mathrm{subst}}(\theta)} = \frac{\rho_{\mathrm{overl}} \times \frac{\mathrm{d}\sigma_{\mathrm{overl}}}{\mathrm{d}\Omega} \times \Lambda_e^{\mathrm{overl}}(E_{\mathrm{overl}})}{\rho_{\mathrm{subst}} \times \frac{\mathrm{d}\sigma_{\mathrm{subst}}}{\mathrm{d}\Omega} \times \Lambda_e^{\mathrm{subst}}(E_{\mathrm{subst}})} \times \frac{1 - \mathrm{e}^{\frac{-t}{\Lambda_e^{\mathrm{overl}}(E_{\mathrm{overl}})\cos\theta}}}{\mathrm{e}^{\frac{-t}{\Lambda_e^{\mathrm{overl}}(E_{\mathrm{subst}})\cos\theta}}} \quad (2)$$

where ρ is the density of atoms per unit volume. Since the P 2p photoelectrons used for characterization originate from the substrate and oxide layer and have the same kinetic energy, equation (2) can be simplified for t as:

$$t = \Lambda_e^{\mathrm{overl}}(E_{\mathrm{overl}}) \times \cos\theta \times ln\left(\frac{N_{\mathrm{overl}}(\theta)}{N_{\mathrm{subst}}(\theta)} \times \frac{\rho_{\mathrm{subst}} \times \Lambda_e^{\mathrm{subst}}(E_{\mathrm{subst}})}{\rho_{\mathrm{overl}} \times \Lambda_e^{\mathrm{overl}}(E_{\mathrm{overl}})} + 1\right) \quad (3)$$

We have verified this quantification approach in numerous circumstances with different surfaces [32–35].

3. Results and discussions

3.1. 5% O_2/Ar treatment (oxygen treatment)

Figure 2 shows the evolution of the O 1s and P 2p core-level spectra following exposure of the freshly cleaved BP surface to 5% O_2/Ar at 20 °C for 10, 70, and 310 min. The exposures were done in the reaction cell and the sample was transferred under UHV conditions without exposure to air. The intensity of the O 1s peak gradually increases with time. Three components could be detected in the O 1s spectra: O(I)—532.2 eV, O(II)—533.5 eV and O(III)—530.9 eV. The freshly cleaved BP shows the P 2p spin-orbital splitting doublet with the P $2p_{3/2}$ peaks at 130.0 eV. There is no peak or shoulder detected at higher BEs confirming that no BP oxidation occurred after cleaving in the glove box. Following the oxygen exposure, two weak P $2p_{3/2}$ peaks centered at 133.9 and 131.7 eV appeared, as shown in the inset of figure 2(b). These peaks grew with increasing the treatment time, representing two oxidation states of phosphorus. The detailed peak assignment and chemical mechanism are discussed below.

3.2. 2.3% H_2O/Ar treatment (water treatment)

Similar to the experiment described above, freshly cleaved BP was exposed to 2.3% H_2O/Ar at 20 °C for 10, 70, and 310 min. Figure 3 shows the O 1s and P 2p core-level spectra obtained following these treatments. The surface species formed in the reaction of BP with water are different from those observed after the oxygen treatment. Thus, the O 1s peak demonstrated two components at 532.7 and 534.0 eV and a single high BE P $2p_{3/2}$ component at 134.5 eV was detected. These facts unambiguously indicate that the surface chemistry of BP is different with water or oxygen. Typically, phosphorus can have the oxidation states of +3 or +5. Most

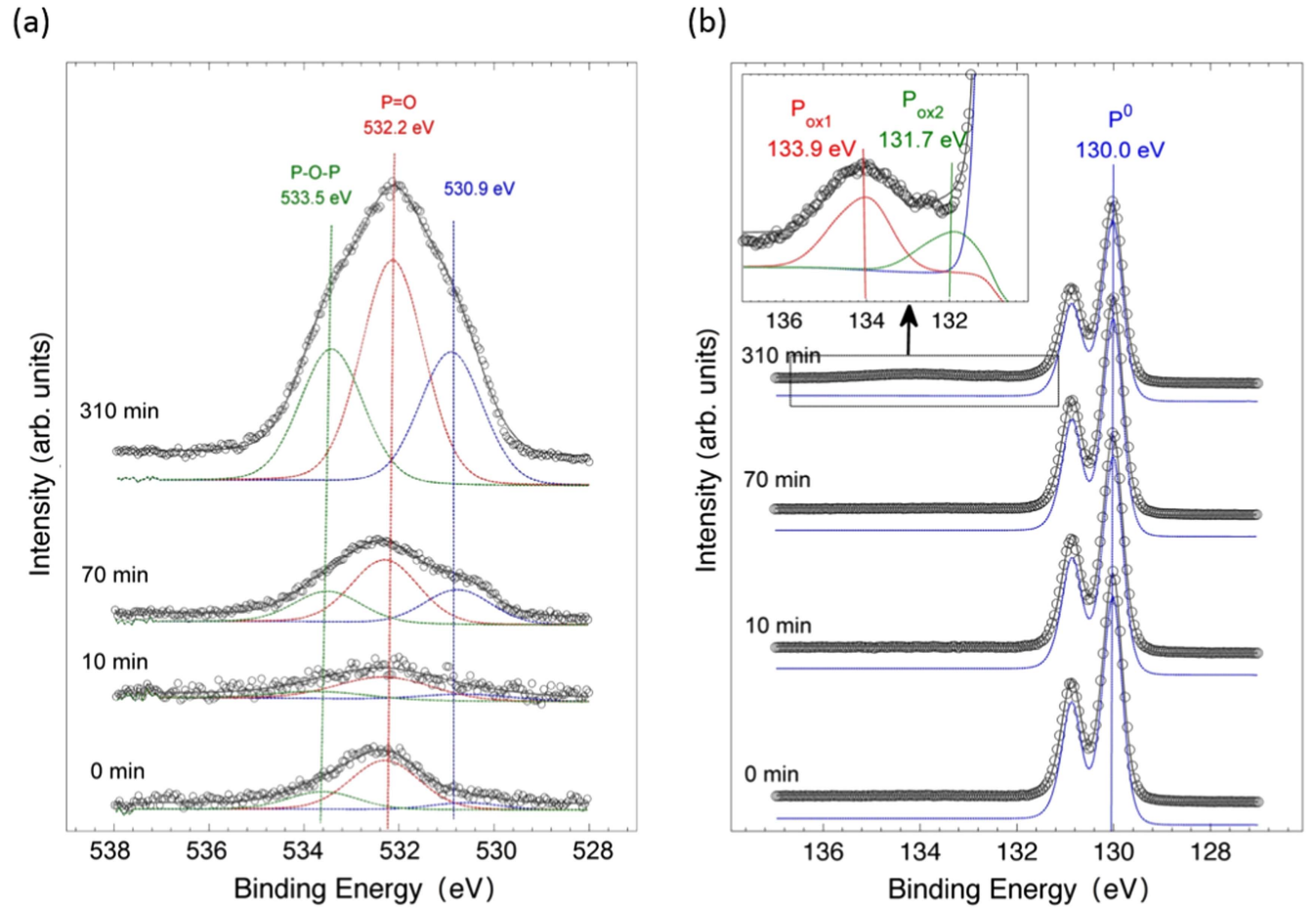

Figure 2. (a) O 1s and (b) P 2p peaks obtained from a freshly cleaved BP surface following exposure to 5% O_2/Ar at 20 °C for 10, 70 and 310 min. The inset of the right panel is a magnification of the high BE region of the top spectrum.

probably, a possible oxidation BP process in water is

$$2\,P + 8\,H_2O \rightarrow 2\,H_3PO_4 + 5\,H_2\nearrow. \quad (4)$$

Therefore, the P $2p_{3/2}$ component at 134.5 eV can be assigned H_3PO_4 (oxidation state = +5). The major O 1s component at 532.7 eV should be due to the OH groups of the H_3PO_4 molecule. Formally, phosphoric acid molecule has P=O bond, the O 1s peak for this chemical state is expected at ~532.2 eV and, therefore, it might be 'screened' by the intensive OH peak. The other component at ~534.0 eV most likely represents a bridge oxygen, P–O–P, this state might form due to H_3PO_4 partial dehydrogenation. XPS BE and its assignment are summarized in table 1.

3.3. 5% O_2 and 2.3% H_2O/Ar mixture treatment (mixture treatment)

Figure 4 shows the O 1s and P 2p core-level spectra obtained following the exposure of a freshly cleaved BP to 5% O_2 and 2.3% H_2O/Ar mixture at 20 °C for 10, 70, and 130 min. The most remarkable difference with the previously described individual treatment in water vapor and oxygen is the much higher oxidation rate. Following the 130 min 'wet oxygen' treatment, an intense peak of oxidized phosphorus was detected (the P $2p_{3/2}$ peak at 134.5 eV). The intensive O 1s peak was characterized by two components at 532.2 and 533.8 eV. The O 1s and P 2p signature unambiguously point to the bulk P_4O_{10} phase. Thus, Wang *et al* [36] had previously reported the P $2p_{3/2}$ peak at 135.0 eV and the O 1s peaks at ~532.5 and ~534.0 eV for phosphorus pentoxide (phosphorus oxidation state = +5). Molecule P_4O_{10} consists of four equivalent phosphorus atoms, four oxygen atoms double-bonded to a phosphorus atom and six oxygen atoms in a bridge position between two phosphorus atoms. Therefore, the O 1s peak should be consistent with two components for P=O and P–O–P with the ratio 4:6. The BE value of P=O component should have lower magnitude (~532.5 eV), compared to the P–O–P component (~534.0 eV). It is remarkable that the curve fitting (figure 4) gives the contributions of 40% and 60% for the P=O and P–O–P components, respectively. This is very different to those observed following only oxygen and only water vapor exposure. Moreover, the ratio between oxygen and the oxidized phosphorus was 0.38, which is very close to that ideally expected for P_4O_{10}.

We noted some similarities in the phosphorus oxidation states and the oxygen states observed following 'dry oxygen'

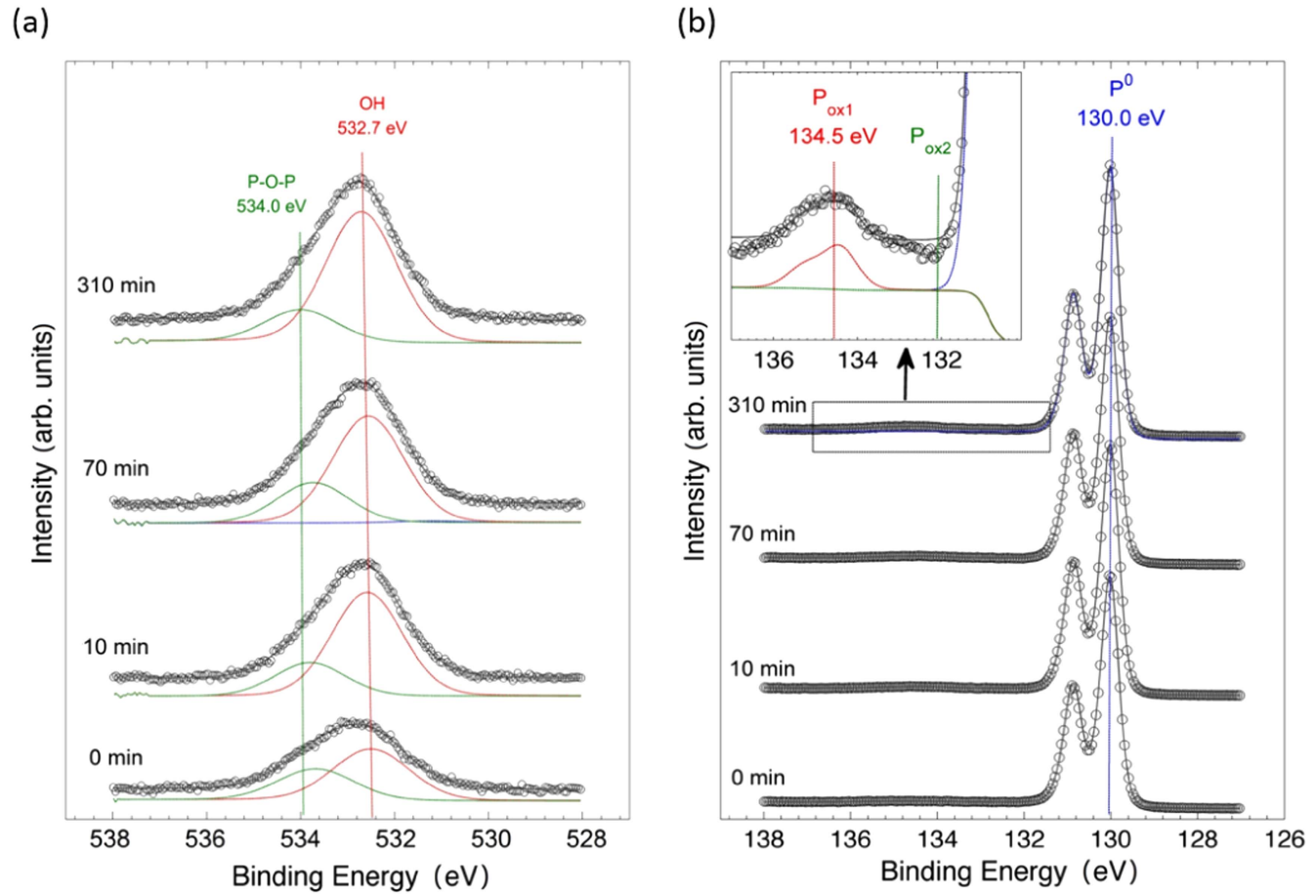

Figure 3. (a) O 1s and (b) P 2p peaks obtained from a freshly cleaved BP surface following exposure to 2.3% H_2O/Ar at 20 °C for 10, 70 and 310 min. The inset of the right panel is a magnification of the high BE region of the top spectrum.

treatment for 310 min and wet oxygen treatment for 10 min. Under both conditions, the P=O component (~532.5 eV) dominated in the O 1s spectra and the component at 530.9 eV was observed. In the P 2p region, two oxidation states were detected as components at 131.7 and ~134 eV. The P $2p_{3/2}$ component at 131.7 eV and the O 1s component at 530.9 eV could be assigned to a surface oxide with the oxidation state less than +5. Phosphorus oxides can have intermediate structures between P_4O_{10} (oxidation state = +5) and P_4O_6 (oxidation state = +3), such as P_4O_9, P_4O_8, and P_4O_7. Normally, a lower oxidation state should be characterized by lower BE. Therefore, the P $2p_{3/2}$ component at 131.7 eV could be fairly attributed to P^{3+} or P^{x+} ($x < 5$). Our hypothesis is that the O 1s peaks at 530.9 and P $2p_{3/2}$ at 131.7 eV could be due to a surface phosphorus oxide. The low BE could be multi-coordinated oxygen in a hollow site. It is likely that, during the treatment in pure oxygen, the formation of the bulk P_4O_{10} phase is kinetically or even thermodynamically hindered, because of the surface passivation towards oxygen dissociation. Water lifts these limitations. The oxidation process includes water interaction with the oxidized phosphorus surface. In the case of phosphorus pentoxide (P_4O_{10}), the following reaction is possible:

$$P_4O_{10} + 6\,H_2O \rightarrow 2\,H_3PO_4. \quad (5)$$

We assume that a similar reaction occurs with the surface oxide and water. The formation of the orthophosphoric acid-like species or phosphoric acid anhydride like $HPO(OH)_2$ species 'free' the surface for oxygen dissociation.

Quantification analysis of the XPS data in terms of oxygen coverage and P_4O_{10} thickness allow better understanding of the kinetics details of the oxidation. As shown in figure 5, the presence of water and oxygen accelerated the phosphorus oxidation greatly. The oxygen coverage obtained in the water atmosphere saturates after 70 min, indicating that the surface was poisoned towards water dissociation. In oxygen, the oxygen coverage picks up more slowly than in the 2.3% H_2O/Ar mixture. However, after 310 min the oxygen coverage is approximately equal in 5% O_2/Ar and in 2.3% H_2O/Ar. In order to estimate the electron attenuation length, we have to make an assumption that all oxide is phosphorus pentoxide. The oxide thickness is calculated, as shown in figure 5(b). The estimated P_4O_{10} thickness shows slow growth and it is less than 5 Å after 310 min in 5% O_2/Ar and in 2.3% H_2O/Ar. In contrast, in the 5% O_2 and 2.3% H_2O/Ar mixture, the oxide reached a 30 Å thickness for 130 min. The 5% O_2 and 2.3% H_2O/Ar mixture has demonstrated itself to be a very strong oxidant.

Table 1. XPS BE and its assignment to different chemical states.

Chemical state	Binding energy, eV		Treatment conditions	Refs.
	O 1s	P $2p_{3/2}$		
P_2O_5/P_4O_{10}	~532.5 ~534.0	135	ambient	[36, 39]
P_4O_{10}	532.2	134.5	5% O_2/2.3% H_2O/Ar mixture after 130 min	This work
	533.8		5% O_2/Ar	
Surface oxide, P^{3+} or P^{x+} ($x < 5$)	530.9	131.7	5% O_2/Ar	
	532.2		5% O_2/2.3% H_2O/Ar mixture after 10 min	This work
Orthophosphoric acid-like H_3PO_4 and/or phosphoric acid anhydride-like ($HPO(OH)_2$)	532.7	134.5	2.3% H_2O/Ar mixture	This work
	534			

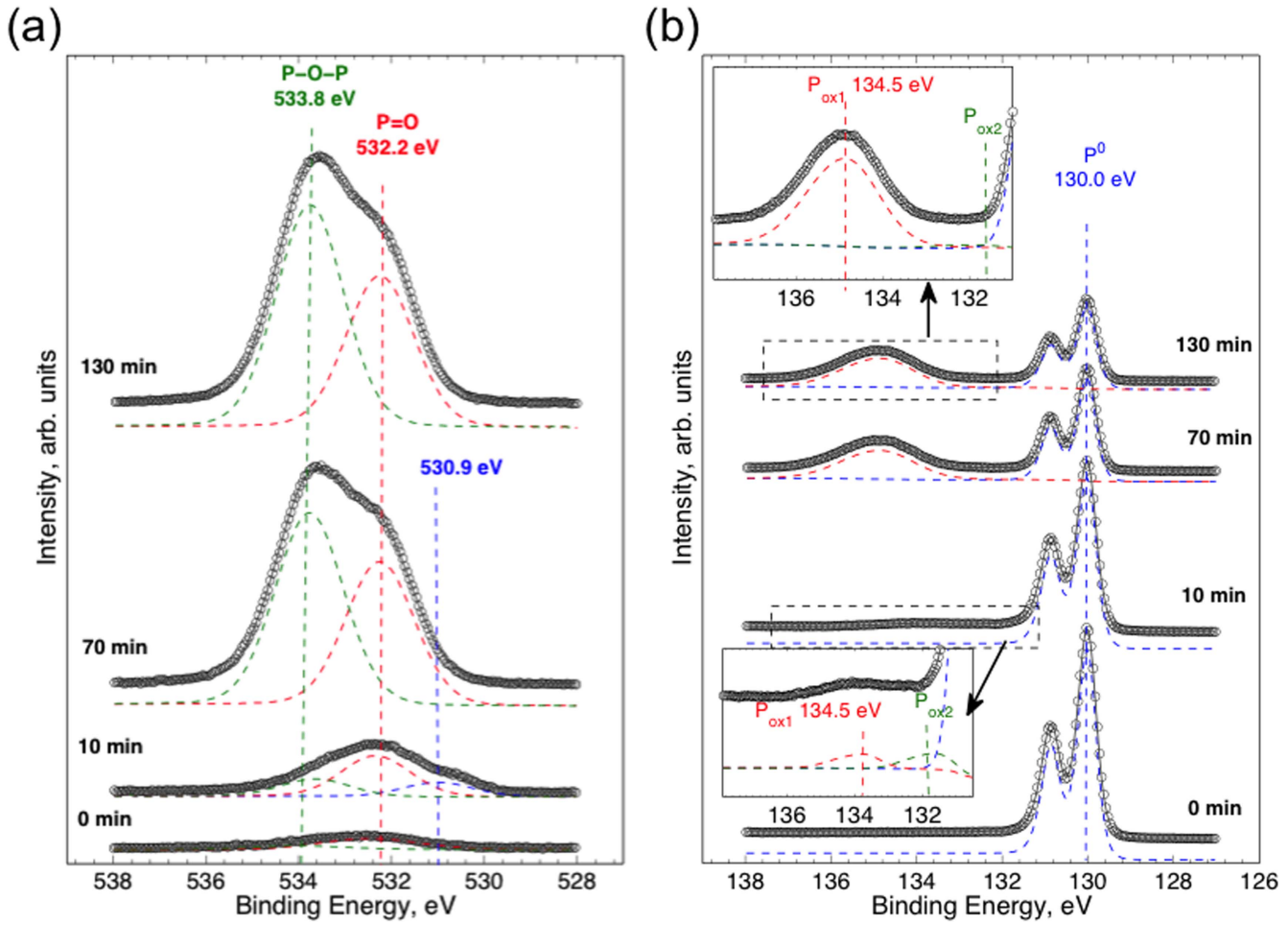

Figure 4. (a) O 1s and (b) P 2p peaks obtained from a freshly cleaved BP surface following exposure to 5%O_2/2.3%H_2O/Ar at 20 °C for 10, 70 and 130 min. The two insets of the right panel are the magnification of the high BE region of the top spectrum and 10 min spectrum, respectively.

3.4. Electrical measurements

The aforementioned XPS studies have proved that water plus oxygen are found to be much more reactive in BP oxidation compared to individual O_2 and H_2O. To examine how to protect BP from oxidation, we have performed electrical measurements of few-layer BP devices with respect to different ALD growth recipes. The conventional ALD system is not a UHV system and usually has a certain level of oxygen.

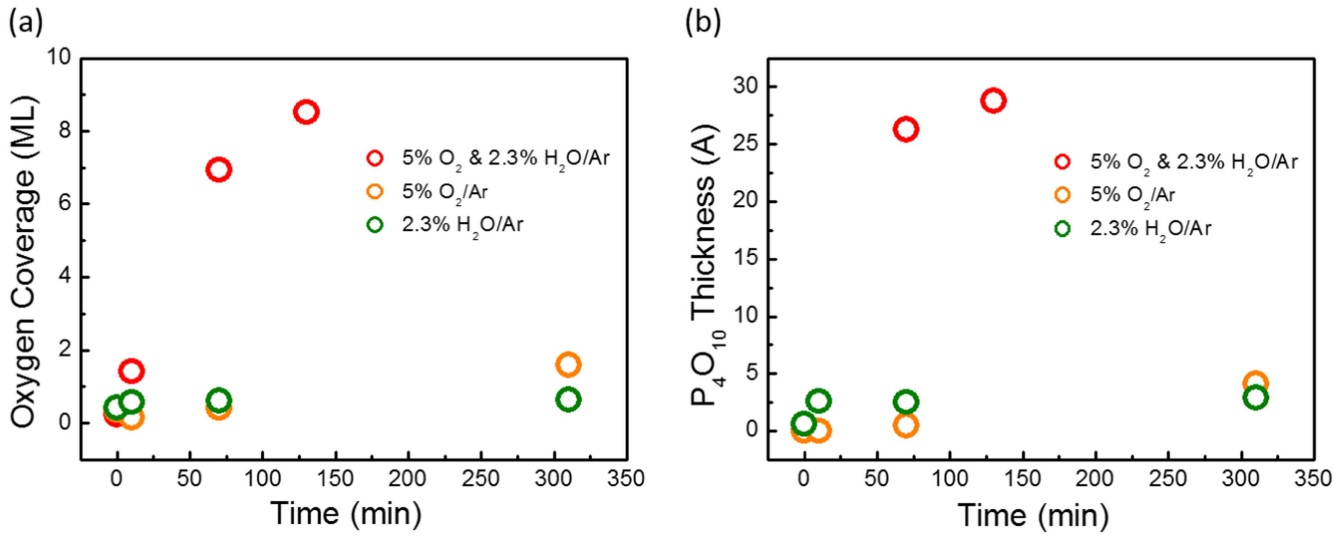

Figure 5. (a) Oxygen coverage and (b) P_4O_{10} thickness change with time for all three different oxidative environments.

Water is widely used as an oxidant precursor for the ALD process. The standard ALD process, i.e. for Al_2O_3, is even at elevated temperatures of 250 °C–300 °C. BP flake was originally exfoliated from bulk BP crystal using the standard scotch tape method, and then transferred to a heavily doped silicon substrate with a 90 nm SiO_2 oxide layer. Prior to device fabrication, the BP film was soaked in acetone for 2 h to remove the tape residue, and then followed with a methanol and isopropyl alcohol (IPA) rinse process. Subsequently, source/drain metal contacts were formed by e-beam lithography with a moderate channel length of 1 μm, metal deposition of 70 nm Ni/Au, and lift-off processes. The schematic view of back-gate modulated BP FET is shown in figure 6(a). ALD Al_2O_3 was deposited after the fabrication of the back-gate modulated BP FET to form BP passivation from the top. To secure a uniform dielectric layer without contacting with water, a 0.8 nm Al layer was pre-deposited prior to the ALD process, as shown in figure 6(b). The Al layer was oxidized in atmosphere and served as a protective layer, which would significantly reduce the possibility of excessive contact between the BP and water even at elevated growth temperatures. Afterwards, a 15 nm Al_2O_3 layer was deposited with trimethylaluminum (TMA) and water as precursors at 200 °C, and the final device structure is presented in figure 6(c). Meanwhile, as a comparison experiment shown in figure 5(d), a 15 nm Al_2O_3 layer was directly deposited with TMA and water at 200 °C, which is similar to the XPS studies under moisture condition. Electrical measurements were carried out upon the devices in air with a Keithley 4200 semiconductor parameter analyzer.

In order to have a fair comparison with our comparison experiment, BP devices with similar thickness and crystal orientation were carefully selected, fabricated and measured. The transfer curves of the devices measured at −0.01 and −0.5 V drain bias are shown in figure 7(a). The transistors show a clear switching behavior with a moderate current on/off ratio of $\sim 10^4$, due to the relatively low band gap of few-layer BP compared to the TMDs. It is interesting that the threshold voltages for the w/ and w/o protective layer are 36.6 and 21.8 V, respectively. The shifted threshold voltage with a magnitude of 14.8 V may be fairly attributed to the light n-type doping effect upon water molecules on the BP FETs, and this effect is widely reported in many 2D materials, such as graphene [37], and MoS_2 [38]. The shift in threshold voltage also confirms the sensitivity of water molecules upon ALD integration on BP, where the w/ and w/o protective layer BP FETs have different electrical characteristics. Inspecting the transfer characteristics of the BP transistors, we can extract the peak transconductance from the linear scale of the transfer curves. The peak transconductance for the w/ and w/o protective layer BP FETs are 59.9 and 7.3 μS mm^{-1} at $V_{ds} = -0.01$ V. We should note that, prior to device fabrication, BP samples with similar thickness have been predetermined by polarized Raman spectroscopy [16], and only those with the same principal axes are chosen to be investigated. This suggests that the quality of BP flakes in the same transport direction before device fabrication are very close, and the significant reduction in transconductance after ALD integration is directly attributed to the Al_2O_3 growth mechanism, which further qualitatively supports our results from XPS studies. Water molecules, coming from the ALD precursor, degrade the quality of the BP channel, resulting in a reduced transport mobility because field-effect mobility is proportional to transconductance. New ALD processes using water-free or oxygen-free oxidants need to be developed. *I–V* output characteristics of BP FETs with and without protective layers are shown in figure 7(b) with a back-gate sweep from +30 V to −30 V and a step of −10 V. On-state current increases as the back gate sweeps from positive voltage to negative voltage, which is a clear signature of p-type transistor behavior. The drain current varies linearly with small source/drain biases, demonstrating an Ohmic-like contact resistance at the metal/BP interface with a small Schottky barrier. The variation among on-state current also illustrates the degradation of BP flake after interacting with water.

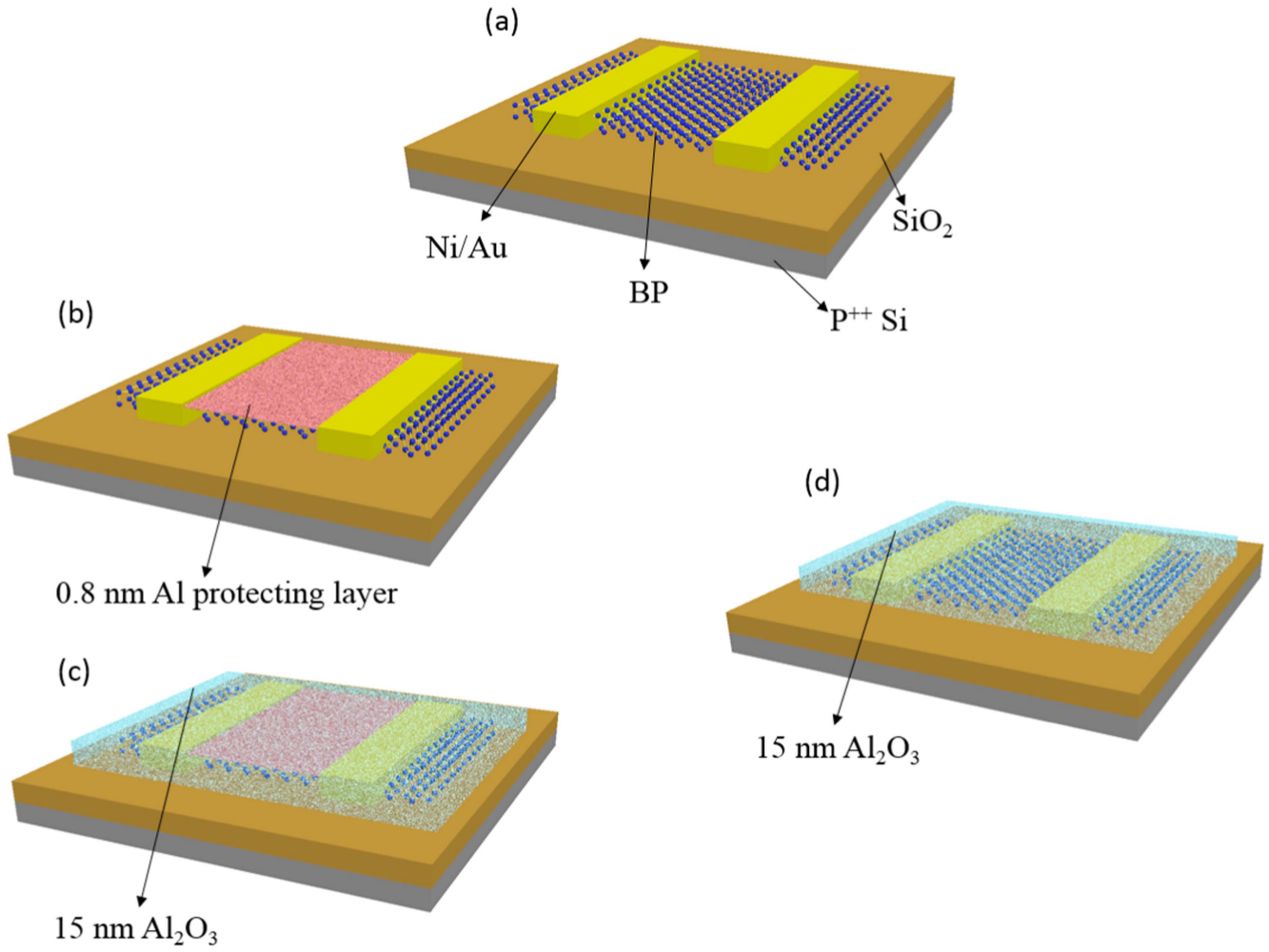

Figure 6. (a) Schematic view of a fabricated back-gate modulated BP FET. (b) Prior to ALD integration on BP, a 0.8 nm Al protective layer was pre-deposited on the BP surface and we waited to oxidize it in ambient conditions. (c) A 15 nm Al_2O_3 layer was then deposited with TMA and water as precursors at 200 °C. (d) A 15 nm Al_2O_3 layer was directly deposited with TMA and water as precursors at 200 °C without applying a 0.8 nm Al protective layer.

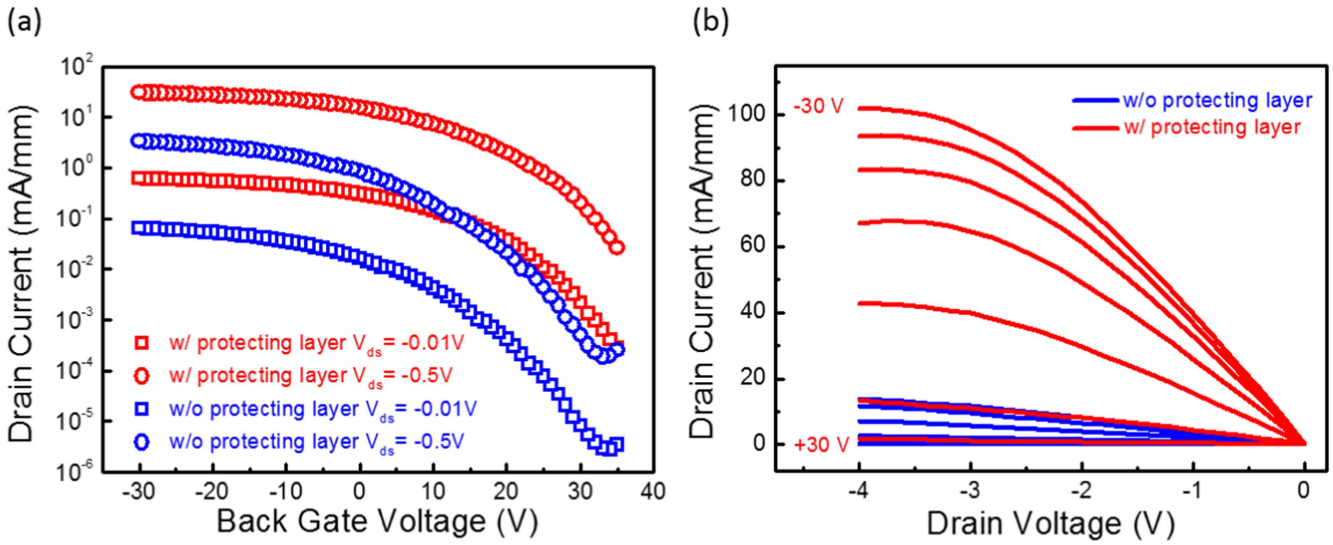

Figure 7. (a) Transfer and (b) output characteristic of BP FETs with two different ALD integration mechanisms.

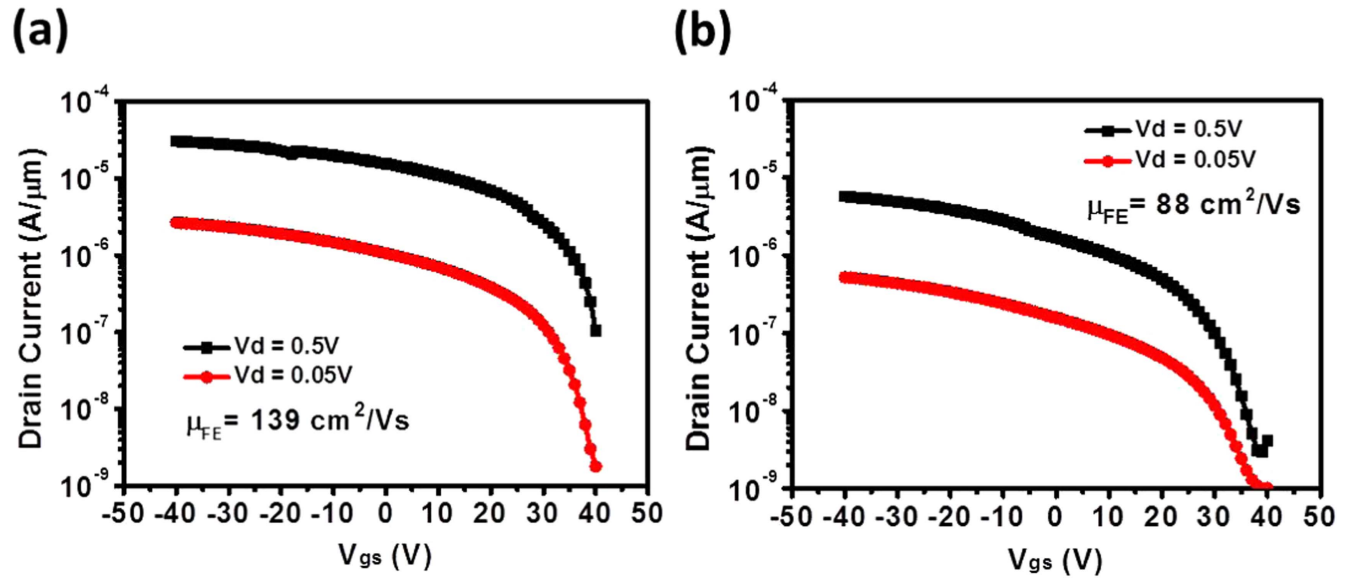

Figure 8. Transfer characteristics of BP FETs fabricated on the same BP flake (a) with h-BN passivation and (b) without passivation.

Figure 8 shows another comparison experiment with or without h-BN passivation. The h-BN is a 2D insulator with a band gap of 6.0 eV and is widely used as gate dielectric or passivation layers for graphene, TMDs, and BP research. Here, we fabricated two 3 μm channel length FETs on the same BP flake with one covered with h-BN and another without any passivation. The h-BN flake is aligned to the BP active region by a dry transfer process inside a glove box with an oxygen and water level of less than 0.1 ppm. Other fabrication steps are similar to what is described above. The devices were measured after 1 d storage in dry nitrogen and less than 1 h exposed to air, as shown in figure 8. The device with h-BN passivation has much higher drain current and an estimated field-effect mobility of 139 $cm^2 V^{-1} s^{-1}$. The transport properties for the naked BP FET are degraded during fabrication and storage with a reduced field-effect mobility of 88 $cm^2 V^{-1} s^{-1}$ and a lower drain current. The h-BN passivated device has similar electrical properties after 1 week storage in dry N_2. The naked device starts to degrade significantly after a long storage time. The experiment offers similar information, that oxygen and water in the fabrication process and in storage are the main sources that degrade the quality of the BP films.

4. Conclusions

BP oxidation was characterized after treatments in 5% O_2/Ar, 2.3% H_2O/Ar, and 5% O_2 and 2.3% H_2O/Ar at 20 °C. 5% O_2 and 2.3% H_2O/Ar is very reactive and results in phosphorus pentoxide of >30 Å for 130 min. Neither water nor oxygen is even close to this reactivity. It is likely that water accelerates the oxidation through the reaction with the surface oxide and thus creates the sites for oxygen dissociation. The BP few-layer FET with a 0.8 nm Al protective layer has presented a better device performance than the one that is directly deposited with TMA and water. Similarly, h-BN passivation also helps retain the good transport properties of BP. Our results provide guidance to preserve the BP sample in a moisture-free environment, as well as engineer ALD integration using water-free precursors.

Acknowledgments

This material is based upon work supported by the US National Science Foundation (ECCS-1449270), AFOSR/NSF EFRI 2DARE Program, Army Research Office (W911NF-14-1-0572), SRC GRC Program. We are grateful for the support of the Birck Nanotechnology Center through the Kirk Grant. W L would like to thank the China Scholarship Council for funding his stay at Purdue University.

References

[1] Liu H, Neal A T, Zhu Z, Luo Z, Xu X, Tomanek D and Ye P D 2014 Phosphorene: an unexplored 2D semiconductor with a high hole mobility *ACS Nano* **8** 4033–41
[2] Li L, Yu Y, Ye G J, Ge Q, Ou X, Wu H, Feng D, Chen X H and Zhang Y 2014 BP field-effect transistors *Nat. Nanotechnol.* **9** 372–7
[3] Xia F, Wang H and Jia Y 2014 Rediscovering black phosphorus as an anisotropic layered material for optoelectronics and electronics *Nat. Commun.* **5** 4458
[4] Gomez A *et al* 2014 Isolation and characterization of few-layer BP *2D Mater.* **1** 025001
[5] Koenig S P, Doganov R A, Schmidt H, Neto A H C and Ozyilmaz B 2014 Electrical field effect in ultra-thin BP *Appl. Phys. Lett.* **104** 103106
[6] Liu H, Du Y, Deng Y and Ye P D 2015 Semiconducting black phosphorus: synthesis, transport properties and electronic applications *Chem. Soc. Rev.* **44** 2732–43
[7] Warschauer D 1963 Electrical and optical properties of crystalline BP *J. Appl. Phys.* **34** 1853–60

[8] Nishii T, Maruyama Y, Inabe T and Shirotani I 1987 Synthesis and characterization of BP intercalation compounds *Synth. Met.* **18** 559–64

[9] Narita S *et al* 1983 Electrical and optical properties of BP single crystals *Physica* B **117–118** 422–4

[10] Baba M, Nakamura Y, Takeda Y, Shibata K, Morita A, Koike Y and Fukase T 1992 Hall effect and two-dimensional electron gas in BP *J. Phys. Condens. Matter* **4** 1535–44

[11] Maruyama Y, Suzuki S, Kobayashi K and Tanuma S 1981 Synthesis and some properties of BP single crystals *Physica* B **105** 99–102

[12] Morita A 1986 Semiconducting BP *Appl. Phys.* A **39** 227–42

[13] Du Y, Liu H, Deng Y and Ye P D 2014 Device perspective for BP field-effect transistors: contact resistance, ambipolar behavior, and scaling *ACS Nano* **8** 10035–42

[14] Du Y, Neal A T, Zhou H and Ye P D 2016 Weak localization in few-layer black phosphorus *2D Mater.* **2** 011001

[15] Deng Y, Luo Z, Conrad N J, Liu H, Gong Y, Najmaei S, Ajayan P M, Lou J, Xu X and Ye P D 2014 BP-monolayer MoS_2 van der Waals heterojunction p-n diode *ACS Nano* **8** 8292–9

[16] Luo Z, Maassen J, Deng Y, Du Y, Garrelts R, Lundstrom M S, Ye P D and Xu X 2015 Anisotropic in-plane thermal conductivity observed in few-layer black phosphorus *Nat. Commun.* **6** 9572

[17] Li L *et al* 2015 Quantum oscillations in a two-dimensional electron gas in black phosphorus thin films *Nat. Nanotechnol.* **10** 608–13

[18] Gillgren N *et al* 2015 Gate tunable quantum oscillations in air-stable and high mobility few-layer phosphorene heterostructures *2D Mater.* **2** 011001

[19] Chen X *et al* 2015 High-quality sandwiched black phosphorus heterostructure and its quantum oscillation *Nat. Commun.* **6** 7315

[20] Cao Y *et al* 2015 Quality heterostructures from two-dimensional crystals unstable in air by their assembly in inert atmosphere *Nano Lett.* **8** 4914–21

[21] Du Y, Liu H, Neal A T, Si M and Ye P D 2013 Molecular doping of multilayer MoS_2 field-effect transistors: reduction in sheet and contact resistances *IEEE Electron Device Lett.* **34** 1328–30

[22] Wood J D, Wells S A, Jariwala D, Chen K S, Cho E, Sangwan V K, Liu X, Lauhon L J, Marks T J and Hersam M C 2014 Effective passivation of exfoliated black phosphorus transistors against ambient degradation *Nano Lett.* **14** 6964–70

[23] Zhu H, McDonnell S, Qin X, Azcatl A, Cheng L, Addou R, Kim J, Ye P D and Wallace R M 2015 Al_2O_3 on black phosphorus by atomic layer deposition: an *in situ* interface study *ACS Appl. Mater. Interfaces* **7** 13038–43

[24] Zhu H, Qin X, Azcatl A, Addou R, McDonnell S, Ye P D and Wallace R M 2015 Surface and interfacial study of half cycle atomic layer deposited Al_2O_3 on black phosphorus *Microelectron. Eng.* **147** 1–4

[25] Island J O, Steele G A, Zant H and Gomez A C 2015 Environmental instability of few-layer black phosphorus *2D Mater.* **2** 011002

[26] Ziletti A, Carvalho A, Campbell D K, Coker D F and Castro Neto A H 2015 Oxygen defects in phosphorene *Phys. Rev. Lett.* **114** 046801

[27] Edmonds M T, Tadich A, Carvalho A, Ziletti A, O'Donnell K M, Koenig S P, Coker D F, Ozyilmaz B, Castro Neto A H and Fuhrer M S 2015 Creating a stable oxide at the surface of black phosphorus *ACS Appl. Mater. Interfaces* **7** 14557–62

[28] Zhang C D, Lian J C, Yi W, Jiang Y H, Liu L W, Hu H, Xiao W D, Du S X, Sun L L and Gao H J 2009 Surface structures of black phosphorus investigated with scanning tunneling microscopy *J. Phys. Chem.* C **113** 18823–6

[29] Fadley C S 1978 Basic concepts of x-ray photoelectron spectroscopy *Electron Spectroscopy: Theory, Techniques and Applications* ed C R Brundel and A D Baker vol 2 (New York: Academic)

[30] Scofield J H 1976 Hartree-Slater subshell photoionization cross-section at 1254 and 1487 eV *J. Electron Spectrosc. Relat. Phenom.* **8** 129–37

[31] Yeh J and Lindau I 1985 Atomic subshell photoionization cross sections and asymmetry parameters: $1 \leqslant Z \leqslant 103$ *At. Data Nucl. Data Tables* **32** 1–155

[32] Gharachorlou A, Detwiler M D, Gu X K, Mayr L, Klötzer B, Greeley J, Reifenberger R G, Delgass W N, Ribeiro F H and Zemlyanov D Y 2015 Trimethylaluminum and oxygen atomic layer deposition on hydroxyl-free Cu (111) *ACS Appl. Mater. Interfaces* **7** 16428–39

[33] Gharachorlou A, Detwiler M D, Mayr L, Gu X K, Greeley J, Reifenberger R G, Delgass W N, Ribeiro F H and Zemlyanov D Y 2015 Surface chemistry of trimethylaluminum on Pd(111) and Pt(111) *J. Phys. Chem.* C **119** 19059–72

[34] Gharachorlou A, Detwiler M D, Nartova A V, Lei Y, Lu J L, Elam J W, Delgass W N, Ribeiro F H and Zemlyanov D Y 2014 Palladium nanoparticle formation on TiO_2(110) by thermal decomposition of palladium(II) hexafluoroacetylacetonate *ACS Appl. Mater. Interfaces* **6** 14702–11

[35] Paul R, Reifenberger R G, Fisher T S and Zemlyanov D Y 2015 Atomic layer deposition of FeO on Pt(111) by ferrocene adsorption and oxidation *Chem. Mater.* **27** 5915–24

[36] Wang Y and Sherwood P M A 2002 Phosphorus pentoxide (P_2O_5) by XPS *Surf. Sci. Spectra* **9** 159

[37] Mitoma N, Nouchi R and Tanigaki K 2015 Enhanced sensing response of oxidized graphene formed by UV irradiation in water *Nanotechnology* **26** 105701

[38] Schmidt H, Giustiniano F and Eda G 2015 Electronic transport properties of transition metal dichalcogenide field-effect devices: surface and interface effects *Chem. Soc. Rev.* **44** 7715–36

[39] Shih P Y, Yung S W and Chin T S 1999 FTIR and XPS studies of P_2O_5-Na_2O-CuO glasses *J. Non-Cryst. Solids* **1999** 211–22